ChemComm

ROYAL SOCIETY OF CHEMISTRY

FEATURE ARTICLE

View Article Online
View Journal

Cite this: DOI: 10.1039/d6cc00070c

Controlling product distributions from ethanol electrolysis

Peter G. Pickup

Electrolysis of bioethanol in proton exchange fuel cells has the potential to become an important technology for sustainable production of green hydrogen and platform chemicals. However, the economic competitiveness of the process relative to water electrolysis is uncertain and will depend strongly on the demand for acetic acid, acetaldehyde, and other by-products. Controlling the product distribution is consequently a crucial element for development of ethanol electrolysis technology. This review focuses on the factors that determine product distributions and mechanistic models of the reaction pathways. Most research on catalysts for electrochemical oxidation of ethanol has focused on increasing current densities and selectivity for the complete oxidation to carbon dioxide. However, a viable technology will require valorization of other products to offset the cost of ethanol. It is therefore important to evaluate and compare catalysts based on the net cost of hydrogen production. Fundamental studies of ethanol oxidation in aqueous electrolytes combined with density functional theory models have provided a comprehensive view of pathways and mechanisms, and of the factors that control product distributions. This provides a background for understanding product distributions obtained from electrolysis cells, and ethanol fuel cells. Generally, it has been found that lower ethanol concentrations and higher temperatures favour the complete oxidation of ethanol to carbon dioxide. Production of acetic acid peaks at intermediate concentrations, and exclusive production of acetaldehyde can be obtained at high concentrations. Pure Pt and PtRh catalysts provide the highest selectivity for complete oxidation. Current densities at low potentials can be increased by combining Pt with oxyphilic metals such as Ru and Sn, although this leads to low selectivity for complete oxidation.

Received 5th January 2026,
Accepted 17th April 2026

DOI: 10.1039/d6cc00070c

rsc.li/chemcomm

1. Introduction

Ethanol is currently the most important renewable fuel and is widely used globally as an additive to gasoline.[1] However, ethanol comprises only a small fraction of total transportation fuel and liquid fuel markets, and its use in combustion engines is inefficient. Electrochemical oxidation of ethanol has the potential to increase efficiencies and provide technologies for sustainable production of power and materials.[2,3]

Direct ethanol fuel cells (DEFC), which have a theoretical efficiency of 97%, have been under development for more than 30 years.[4,5] However, progress has been impeded by low performances, low voltage efficiencies, and the production of acetaldehyde and acetic acid by-products.[3,6] Consequently, the focus for development of ethanol based power technologies has shifted to electrolysis of ethanol to produce green hydrogen, with valorisation of the by-products to offset costs.[2,7]

There are three distinct types of ethanol electrolysis cell (EEC) and DEFC that are based on proton exchange membranes (PEM), anion exchange membranes or high-temperature solid oxide separators.[3,6,8] This review is focused on PEM cells because they operate at moderate temperatures and, unlike alkaline cells, do not require a consumable source of OH^-. The primary difference between an EEC and DEFC is that electrical energy is used to generate hydrogen at the cathode instead of reduction of oxygen at a fuel cell cathode to produce electrical power (Fig. 1).[9]

Department of Chemistry, Memorial University of Newfoundland, St. John's, NL A1B 3X7, Canada. E-mail: ppickup@mun.ca

Peter G. Pickup

Peter G. Pickup is a Professor Emeritus and University Research Professor at Memorial University of Newfoundland in Canada. He has worked in diverse areas of chemistry including inorganic and organic materials, chemically modified electrodes, conducting polymers, fuel cells, electrocatalysis, and ethanol electrolysis. He holds a BA and DPhil from Oxford University.

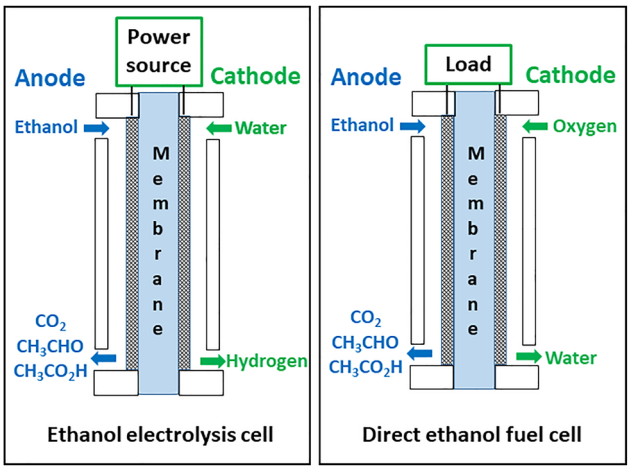

Fig. 1 Schematic diagrams of an ethanol electrolysis cell and direct ethanol fuel cell.

From a practical perspective, stationary production of hydrogen and commodity chemicals at an EEC plant is much more feasible than collecting by-products from mobile DEFC applications,[10] although valorisation of by-products from stationary DEFC applications will also be crucial. The dependence of the cost of hydrogen on commodity prices will make it necessary to vary the product distribution as prices change. This can be achieved by varying the operating conditions (ethanol concentration, cell potential, temperature) and changing the anode catalyst if necessary.[11]

For ethanol electrolysis, the cost of the hydrogen produced will determine economic viability, and will need to be competitive with water electrolysis.[7,11] Fig. 2 shows a comparison of projected hydrogen costs, based on two difference pricing scenarios, for various catalysts, ethanol concentrations, and current densities.[11] In scenario A, based on Jan 2025 prices, the lowest ethanol concentration (0.1 M) with a Pt or PtRu catalyst provides the lowest cost of hydrogen at the lowest current density (and lowest potential). However, a PtRu catalyst with 4 M ethanol provides the best balance between cost and current density, due to the high yield and high price of acetaldehyde. For equal prices of ethanol, acetic acid and acetaldehyde (scenario B) lower ethanol concentrations provide the lowest hydrogen cost and a PtRhRu catalyst provides the optimum performance. Although this cost analysis is conceptual, and lacks a detailed techno-economic model, it provides a crucial framework for comparing catalysts and operating conditions.

Since the cost of hydrogen depends strongly on the value of each product, the selectivity of the process will need to be varied as market prices change.[11] This review is therefore focussed on the factors that determine product distributions from electrochemical oxidation of ethanol, with an emphasis on products from ethanol electrolysis in PEM cells. In addition, electrochemical and computational models developed from the extensive body of work on the electrochemical oxidation of ethanol in aqueous acid electrolytes are reviewed to provide a framework for optimization of catalysts and operating condition.

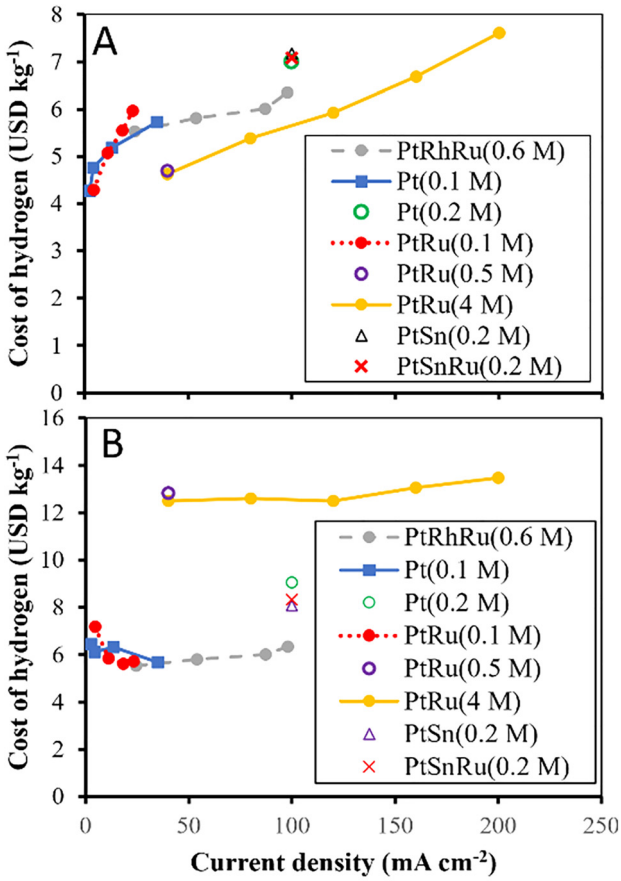

Fig. 2 Comparison of the projected cost of hydrogen from electrolysis of ethanol at various catalysts, ethanol concentrations and current densities. Scenario A is based on Jan 2025 prices of 0.53 USD kg^{-1} for ethanol, 0.50 USD kg^{-1} for acetic acid and 0.98 USD kg^{-1} for acetaldehyde, while scenario B is based on equal prices of 0.50 USD kg^{-1} for these commodities. Reproduced from ref. 11. Copyright © 2025 American Chemical Society.

2. Reactions and products

Complete oxidation of ethanol to carbon dioxide (eqn (1)) generates 12 electrons (n = 12), which provides the maximum faradaic efficiency (and fuel efficiency) for a fuel cell[12] and maximum yield of hydrogen in an electrolysis cell.[11,13]

$$CH_3CH_2OH + 3H_2O \rightarrow 2CO_2 + 12H^+ + 12e^- \quad (1)$$

Although high faradaic efficiencies for CO_2 are obtained at high temperatures in solid oxide cells, and at moderate temperatures in alkaline cells, complete oxidation to CO_2 has not been achieved, and PEM cells predominantly produce acetic acid and acetaldehyde (eqn (2) and (3)).

$$CH_3CH_2OH + H_2O \rightarrow CH_3CO_2H + 4H^+ + 4e^- \quad (2)$$

$$CH_3CH_2OH + H_2O \rightarrow CH_3CHO + 2H^+ + 2e^- \quad (3)$$

The lower number of electrons transferred (*i.e.* lower stoichiometry) decreases fuel efficiency in fuel cells, and selectivity for hydrogen production from ethanol electrolysis. However,

the value of these products, and lower CO_2 emissions, can make the overall process more economical.

A number of other products from electrochemical oxidation of ethanol have been reported, including ethyl acetate,[14,15] ethane,[16] methane,[16] ethane-1,1-diol,[17] and ethoxyhydroxyethane.[17] Ethyl acetate is formed by the chemical reaction (condensation) of acetic acid with ethanol[15,17] and so is treated as electrochemical formation of acetic acid where relevant. Methane and ethane are formed by reduction of adsorbed hydrocarbon residues during potential cycling,[16] and so would not normally be formed during ethanol electrolysis.

3. Measurements of product distributions from ethanol oxidation in aqueous acid electrolytes

The most widely used techniques for analysis of product distributions from electrochemical oxidation of ethanol are Fourier transform infrared spectroscopy (FTIR) and differential electrochemical mass spectrometry (DEMS).[18] These methods have generally been applied at ambient temperature in aqueous electrolytes in order to provide mechanistic information, and so are only briefly reviewed here. However, they have been instrumental in the development of the reaction pathways and mechanisms discussed in Section 8.

FTIR methods have been used to identify and quantify both adsorbed intermediates and products.[19–21] Iwasita and Pastor[22] quantified adsorbed $-C(OH)CH_3$, $-OCH_2CH_3$, $-COCH_3$, and –CO species from ethanol on a Pt electrode, and the number of electrons required to oxidize each species to CO_2. They proposed that –CO is formed from $-C(OH)CH_3$ *via* the $-COCH_3$ intermediate. Wang and Abruna[23] have detected adsorbed enolate, ketene, and vinyl/vinylidene, and proposed a mechanism in which CO_2 is derived from the adsorbed enolate ($CH_2{=}CHO^-_{ads}$) intermediate. In an FTIR study of ethanol oxidation at stepped platinum single crystal electrodes, Colmati *et al.*[24] found that (110) steps on (111) terraces promote both C–C bond cleavage and oxidation of adsorbed CO (CO_{ads}) at low potentials. In contrast, (100) steps were only effective at high potentials.

DEMS, in which the electrochemical cell is interfaced to a mass spectrometer, provides quantitative analysis of volatile products from ethanol oxidation, and has been employed with both liquid and solid electrolytes. Behm and coworker[16,25] reported product distributions for both potentiodynamic and potentiostatic oxidation of ethanol in aqueous 0.5 M sulphuric acid at Pt, PtRu and Pt_2Sn catalysts. The main products were acetaldehyde and acetic acid, with CO_2 representing only 1% of the detected products. In contrast, Bergamaski *et al.*[26] found that Rh and PtRh catalysts were much more efficient than Pt for the CO_2 formation from 0.1 M ethanol in 0.1 M $DClO_4$(aq) during potential cycling, but not at constant potential. More recent studies have further elucidated the important roles that Rh can play in ethanol oxidation.[27–31]

Most FTIR and DEMS studies of ethanol oxidation have been performed at ambient temperature, and so have limited relevance to ethanol electrolysis in PEM cells, which are usually operated at 80 °C. However, a notable study by Sun *et al.*[32] employed a high temperature and pressure DEMS cell over a range of temperatures and ethanol concentrations. Oxidation of ethanol to CO_2 in aqueous H_2SO_4 was enhanced at higher temperatures, lower ethanol concentrations and lower potentials, with *ca.* 90% current efficiency for CO_2 formation at 100 °C, 0.01 M, and 0.48 V *vs.* RHE.

4. Influence of the timescale employed for measurement of product distributions

Although FTIR and DEMS studies have been instrumental in developing our understanding of ethanol oxidation and reaction mechanisms, their relevance to ethanol electrolysis must be scrutinized. In addition to the effects of temperature, and the use of a solid polymer electrolyte in PEM electrolysis cells, the timescale of the measurements has a huge influence on the measured product distribution. This was clearly demonstrated by online measurement of acetic acid and CO_2 concentrations exiting a EEC (referred to as a DEFC with H_2 at the cathode at the time) at constant current and ambient temperature, using a conductivity cell and non-dispersive infrared (NDIR) CO_2 monitor, respectively.[33] The measured CO_2 concentration increased rapidly to a peak, and then rapidly decreased, while the acetic acid concentration increased to a steady state. The average faradaic efficiency for CO_2 over 1 h was only 1.7% while acetic acid and acetaldehyde were produced with 45% and *ca.* 50% efficiency, respectively. The peak in the apparent efficiency for CO_2 formation at the beginning of the electrolysis was due stripping of CO_{ads} formed before the current was applied.[34]

Piwowar and Lewera[29] have reported a thorough analysis of how stripping of pre-adsorbed CO has influenced reports on the apparent promotion of CO_2 formation by Rh containing catalysts. Their DEMS study employed Pt, Rh, and various PtRh alloy catalysts with 1.2 M ethanol in 0.5 M H_2SO_4(aq), at ambient temperature. Integrated ionic current densities for CO_2 production from ethanol during a single potential cycle were 10–20% lower than those obtained for a pre-adsorbed monolayer of CO in the absence of ethanol and did not vary significantly for the different catalysts. Furthermore, their analysis of data from a DEMS and FTIR study by Delpeuch *et al.*[28] revealed that the amount of CO_2 detected corresponded to less than 50% of a monolayer of CO_{ads}. The clear conclusion is that the whole amount of CO_2 detected during ethanol oxidation can come exclusively from CO_{ads} produced through dissociative adsorption of ethanol before the potential (or current) scan (or step) is applied. Consequently, it is essential that data is corrected to account for this source of CO_2, or steady state data is collected after the effect of the initial CO_{ads} has dissipated. Unless otherwise stated, product distributions in the following sections were obtained during steady state operation of the cell.

5. Measurements of product distributions from ethanol oxidation in DEFC

Since the use of PEM cells for ethanol electrolysis is a relatively new (2010) concept,[35–37] much of the pertinent data on product distributions from ethanol oxidation in PEM cells is from DEFC studies. Anode catalyst overpotentials and product distributions are similar for DEFC and EEC, and so data from DEFC provides good estimates of EEC performance (and *vice versa*) when the difference in cathode potential is accounted for.[38]

Rousseau *et al.*[12] reported the first full, charge balanced analysis of products from a DEFC. Acetic acid, acetaldehyde and CO_2 exiting the cell were collected in a series of traps and analysed by high performance liquid chromatography. For 4 h of electrolysis at 80 °C, a Pt catalyst produced chemical yields (percentage of the ethanol consumed that is converted to each product) of 32.5% acetic acid, 47.5% acetaldehyde and 20% CO_2, while a PtSn catalyst produced 76.9% acetic acid, 15.2% acetaldehyde and 7.7% CO_2. Although, the electrochemical performance (current and power *vs.* potential) was much higher for the PtSn catalyst, it was offset by the lower selectivity for the complete oxidation to CO_2, and this has generally been observed for catalysts in which Pt is combined with other elements. In another example, Wnuk and Lewera[39] reported that a Pt catalyst was much more selective for CO_2 formation than PtRu and that decreasing the ethanol concentration from 0.5 M to 0.25 M significantly increased selectivity towards CO_2 at the Pt catalyst.

Studies of product distributions from DEFC have also shown that it is essential to account for diffusion of reactants and products through the PEM (crossover).[39–41] This is an acute problem in DEFC because it allows ethanol to react chemically with oxygen, and this is impossible to distinguish from electrochemical formation of products. It has been circumvented by supplying N_2 + H_2 or just N_2 to the cathode to run the cell as a EEC,[40] and this has been shown to be the best way to evaluate catalysts for DEFC.[38,42] Nonetheless, crossover of ethanol and products from the anode to the cathode must be accounted for in EEC by analyses of both the anode and cathode exhaust streams.[38]

Wang *et al.*[14] compared performances and product distributions for DEFC (1.5 M ethanol at 90 °C) with PtRu and PtSn catalysts, and with a bilayer anode in which a PtRu layer adjacent to the Nafion membrane was coated with a PtSn layer. Although the bilayer anode provided much higher current and power densities than the single layer anodes, chemical yields for CO_2 and acetic acid formation were $<0.7\%$ and $>73\%$, respectively, in all cases. Andreadis *et al.*[43] reported much higher CO_2 selectivity and lower acetic acid selectivity for a PtRu catalyst at 90 °C with 1 M ethanol, with chemical yields from 8–15% and *ca.* 35%, respectively. Acetaldehyde yields ranged from 49% to 57% and increased at lower temperatures and higher current densities. The CO_2 yield was highest at the highest temperature and lowest current density.

6. Measurements of product distributions from ethanol electrolysis in PEM cells

Table 1 shows a summary of reports that provide full product distributions from PEM EEC. Although differences in conditions make direct comparisons difficult, this data provides an important guide to the effects of the catalyst, temperature and cell potential on the current density and product distribution.

Table 1 Chemical yields of products from selected reports on ethanol electrolysis in PEM cells. Data reported as faradaic efficiencies has been converted to chemical yields

Catalyst	T (°C)	[Ethanol] (M)	Potential (V)	Current density (mA cm^{-2})	Chemical yield (%)			Ref.
					CO_2	Acetic acid	Acetaldehyde	
Pt	20	2	0.92–0.97	100	12	42	46	37
$Pt_{0.9}Sn_{0.1}$	20	2	0.92–0.97	100	29	41	30	37
$Pt_{0.86}Sn_{0.1}Ru_{0.04}$	20	2	0.80–0.96	100	29	32	39	37
Pt	80	0.1	0.50	35	50	46	3	38
PtRu	80	0.1	0.50	23	7	90	4	38
PtSn	80	0.1	0.50	17	26	65	9	38
Pt	80	0.1	0.40	18	27	41	32	38
Pt/PtRu bilayer	80	0.1	0.40	28	31	65	4	44
PtRu 2 : 1	80	4	0.64	80	0	7[a]	93	45
PtRu	80	0.5	0.64	40	0	9	91	15
PtCu	80	4	0.65	40	0	0	100	46
PtCo	80	4	0.62	40	0	0	100	46
PtCo	80	4	1.05	360	0	16[a]	84	46
PtNi	80	4	0.61	40	0	0	100	46
PtRu@$Pt_{1.7}$[b]	80	0.1	0.50	16	28	51	21	47
Ru@$Pt_{1.0}$[b]	80	0.1	0.50	14	21	56	23	48
$Pt_{2.0}Rh$[b]	80	0.1	0.50	18	56	44	0	49
Rh@Pt(2 ML)[b]	80	0.1	0.5	14	47	53	0	50
PtRhNi[b]	80	0.1	0.5	17	64	36	0	51
PtRhRu[b]	80	0.1	0.5	21	42	57	0	51
PtRuRu	80	0.6	0.5	54	15	80	5	11

[a] The yield of ethyl acetate has been added to the acetic acid yield. [b] The cell was operated in crossover mode.

Lamy *et al.*[37] measured acetic acid and acetaldehyde from EEC with Pt, PtSn, and PtSnRh catalysts by chromatography, and calculated the CO_2 yield from the charge balance. The presence of Sn increased CO_2 production and decreased acetaldehyde. Adding Ru decreased acetic acid production.

We developed a methodology in which products from the anode and cathode were collected and analysed separately,[40,42] which was subsequently simplified by combining the anode and cathode exhausts prior to analysis.[38] Acetic acid, acetaldehyde, and residue ethanol were determined by proton nuclear magnetic resonance spectroscopy, while CO_2 was monitored during electrolysis with a NDIR detector. The sum of ethanol plus products exiting the cell was 99.3% of the ethanol entering the cell, indicating that no other products were formed in significant quantities. A comparison of commercial Pt, PtRu, and PtSn catalysts for electrolysis of 0.1 M ethanol at 80 °C showed that selectivity for formation of CO_2 was Pt > PtSn > PtRu, with a maximum of 50% for Pt at 0.5 V. The order was reversed for acetic acid, with a maximum of 93% at 0.7 V. Acetaldehyde yields were highest (57% for Pt and 52% for PtRu) at the lowest potential (0.2 V).

Since PtRu catalysts are much more active than Pt alone for ethanol oxidation at low potentials, but Pt is more selective for the complete oxidation, various combinations of PtRu and Pt catalysts have been employed.[44] A mixture and two bilayer configurations provided higher current densities at potentials from 0.35 V to 0.45 V than each catalyst alone. CO_2 selectivity for the membrane/Pt/PtRu configuration was not significantly different from the selectivity of Pt over this potential range, and therefore provided higher overall efficiency.

De la Osa and coworkers[45] studied the effect of the Pt : Ru mass ratio on electrolysis of 4 M ethanol at 80 °C. A 2 : 1 ratio provided the lowest and most stable operating potentials over a range of current densities from 40–160 mA cm^{-2}. While acetaldehyde was the only product detected by gas chromatography at 40 mA cm^{-2}, increasing amounts of acetic acid were detected at higher current densities. There was good agreement between the rates of production of hydrogen and the detected products, indicating that there was insignificant production of CO_2.

In a subsequent paper using a commercial PtRu catalyst, the de la Osa group varied the ethanol concentration (from 0.5 to 6 M) and studied the formation of ethyl acetate.[15] In all cases (from 40–280 mA cm^{-2}) acetaldehyde was the major product ($\geq$75%) and no CO_2 was detected. Yields of acetic acid peaked at 25% for 1 M ethanol at 120 mA cm^{-2} and decreased at higher concentrations and current densities. Yields of ethyl acetate increased with increasing concentration and current density, reaching *ca.* 4% for 6 M ethanol at 280 mA cm^{-2}.

PtCu, PtCo and PtNi catalysts have been reported to provide 100% yields of acetaldehyde from 4 M ethanol at 80° at 40 mA cm^{-2}.[46] The PtCo catalyst provided stable operation over a 75 min period as the current density was stepped from 200 to 360 mA cm^{-2}. Yields of ethyl acetate were $\leq$3.3% for these catalysts.

Modification of a PtRu catalyst by deposition of a Pt layer onto the surface of the PtRu nanoparticles to form PtRu@Pt core–shell structures provided control over its activity and selectivity.[47] Product distributions for a series of catalysts with different Pt shell thicknesses were determined by operating a PEM electrolysis cell in crossover mode, where ethanol is supplied to the cathode and oxidized at the anode. Diffusion of ethanol through the membrane provides control of the mass transport rate and allows the stoichiometry of the ethanol oxidation reaction to be determined. Combining this with NDIR measurement of the CO_2 yield provides the product distribution. It was found that increasing the Pt coverage decreased activity at low potentials and increased CO_2 yields. A PtRu@$Pt_{1.7}$ catalyst provided a 28% yield of CO_2 (*vs.* 7% for PtRu) from electrolysis of 0.1 M ethanol at 0.5 V and 80 °C. Ru@Pt catalysts also provide enhanced CO_2 selectivity over PtRu and higher current densities than Pt at low potentials.[48]

PtRh alloy[49] and core–shell (Rh@Pt)[50] catalysts are particularly active and provide high CO_2 selectivity. Yields of 56% and 47%, respectively, were obtained in crossover mode for a Pt_2Rh alloy catalyst and a Rh@Pt catalyst with a 2 monolayer (ML) Pt shell. Activity and selectivity were manipulated by varying the Pt : Rh ratio, as illustrated in Fig. 3. The current density at potentials above *ca.* 0.35 V is mass transport controlled, and is proportional to the stoichiometry of ethanol oxidation. Higher currents in this region generally indicate a higher yield of CO_2.

Incorporation of a third metal into PtRh alloy catalysts provides further control over activity and selectivity.[51] A PtRhNi catalyst with a 3 : 1 Pt : Rh ratio provided a higher current density at 0.5 V than the corresponding Pt_3Rh catalyst and the highest CO_2 selectivity (64%) that has been reported to date.

The activity of a PtRhRu catalyst was much higher at low potentials than either PtRh or PtRhNi, and more selective for production of acetic acid.[51] This PtRhRu catalyst is very effective for production of hydrogen and acetic acid in a conventional EEC (Fig. 2 and 4).[11]

Ju *et al.*[53] have reported product distributions from experiments in which the ethanol solution was recycled through the

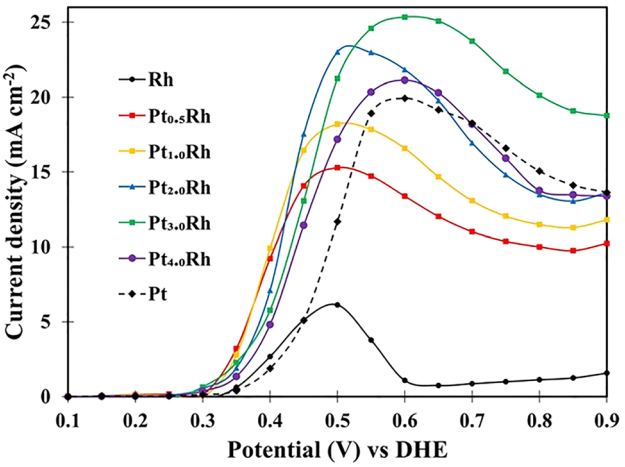

Fig. 3 Polarization curves for electrolysis of 0.1 M ethanol at Rh, PtRh, and Pt catalysts at 80 °C in a PEM electrolysis cell operated in crossover mode. Reproduced from ref. 49. Copyright © 2025 American Chemical Society.

cell. After 4 h of electrolysis of 2 M ethanol at a PtSn catalyst at 70 °C, the main product was acetic acid, with a relatively small amount of acetaldehyde. After 8 h, the concentrations of both had increased significantly and there was a high concentration of ethane-1,1-diol (acetaldehyde hydrate). After 24 h, chemical yields of acetic acid, acetaldehyde, ethane-1,1-diol, and CO_2 were 73%, 6%, 19%, and <2%, respectively.

Product distributions have also been recently reported for PtRu supported on adenine-based noble carbons[52] and Ketjen-black (KB) carbon,[13] PtRu catalysts with varied particle sizes, alloying degree and surface oxidation,[54] and a $PtRuSn_{0.3}$ catalyst.[55]

7. Factors that determine product distributions

It is clear from the data summarised in Table 1, and data from DEFC and aqueous acid electrolytes, that product distributions are determined primarily by the temperature, ethanol concentration, cell potential and anode catalyst. However, unravelling how these factors combine and interact is complex. Generally, higher temperatures favour CO_2 formation.[32,36,39,43,56,57] Most of the data available for PEM ECC has been obtained at 80 °C in order to maximize CO_2 formation, while minimizing membrane and catalyst degradation.

The influence of ethanol concentration is more complex, and is strongly influenced by the cell potential. This is illustrated in Fig. 4 where chemical yields of acetic acid, acetaldehyde, and CO_2 from selected studies are plotted as a function of ethanol concentration. Trends with increasing cell potential are indicated by the arrows and labels. In all cases, except for the PtRhRu catalyst at 0.4–0.5 V, the yield of acetic acid (measured as acetic acid plus ethyl acetate) increased with increasing potential. CO_2 yields increased with potential for 0.1 M ethanol, but generally decreased with potential at higher concentrations. These trends are reversed for acetaldehyde.

It can be seen from the data in Fig. 4 that acetic acid and CO_2 yields generally decrease with increasing ethanol concentration while acetaldehyde yields increase. The notable exceptions are for the PtRhRu catalyst from 0.2–0.6 M ethanol, where acetic acid yields increase and acetaldehyde yields decrease or are variable.

Regarding the effect of the catalyst, it can be seen that PtRu produces very low yields of CO_2 at all concentrations and potentials and very high yields of acetaldehyde at high concentrations. In contrast, the Pt catalyst produced high yields of CO_2 with 0.1 M ethanol, which is the only data available for Pt. PtRuRh approximately follows the trends between the behaviour of Pt at low concentrations and PtRu at high concentrations, but with an anomalously high acetic acid/acetaldehyde selectivity at intermediate concentrations.

Fig. 4 provides an important guide for the selection of catalysts and operating conditions for controlling product distributions. Although the data is limited, understanding the trends with concentration and potential will provide a basis for

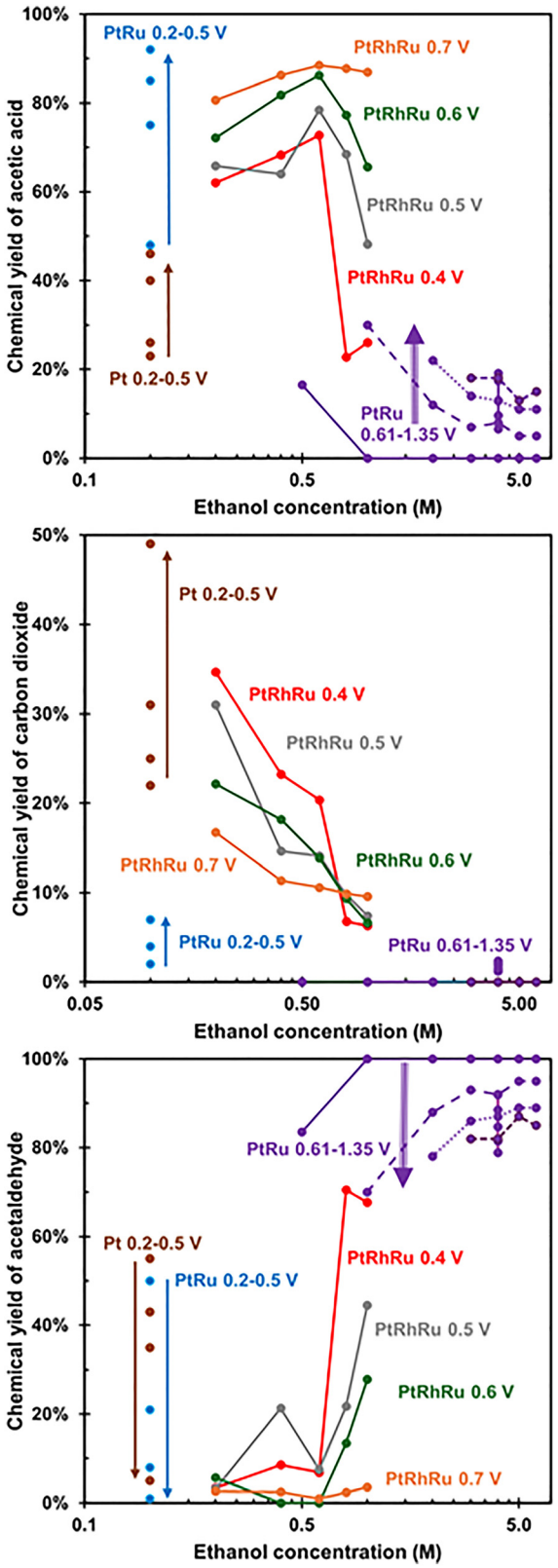

Fig. 4 Chemical yields of acetic acid, carbon dioxide, and acetaldehyde *vs.* ethanol concentration from selected studies (ref. 11, 15, 38 and 52) on product distributions from ethanol electrolysis in PEM cells. Trends with increasing cell potential are indicated by the arrows and labels.

designing catalysts that can be used to minimize the cost of hydrogen as market conditions evolve.

8. Reaction pathways and mechanisms

8.1. Pt catalysts

Our understanding of the reaction pathways and mechanisms for electrochemical oxidation of ethanol at Pt based surfaces has been developed over more than four decades.[18,58] Fig. 5 shows the main pathways to CO_2, acetaldehyde (A), and acetic acid (AA), and the oxidation of water to produce adsorbed –OH required for oxidation of CO_{ads} to CO_2 and CH_3CO_{ads} to acetic acid.[59] Although there are more detailed reaction schemes and mechanisms,[17,60,61] and some variants (*e.g.* for potentiodynamic conditions),[23,62] Fig. 5 provides a suitable summary for this discussion. Sanchez-Monreal *et al.*[59,63] have developed a kinetic model based on this reaction mechanism that provides a link between theoretical models and experimental data.

Understanding of the factors that determing the relative rates of the many processes involved in ethanol oxidation has been developed from computational studies based on density functionional theory (DTF). In 2008, Wang and Liu[64] reported a DFT study of ethanol oxidation at Pt(111), Pt(211), and Pt(100) surfaces using a transition-state searching technique. Adsorbed acetyl (CH_3CO_{ads}), formed *via* CH_3CHOH_{ads} or CH_3CHO, was found to be the key intermediate for breaking the C–C bond to produce CO_2 and other one carbon (C1) products. As long as acetaldehyde produced in the initial step readsorbs onto the surface, it can easily dehydrogenate to CH_3CO_{ads}. A Pt(100) surface provided the most favourable pathway (lowest calculated reaction bariers) from CH_3CO_{ads} to CO_2, which was much more favorable than the hydroxylation to acetic acid. In contrast, acetaldehyde and acetic acid are the dominant products on Pt(111).

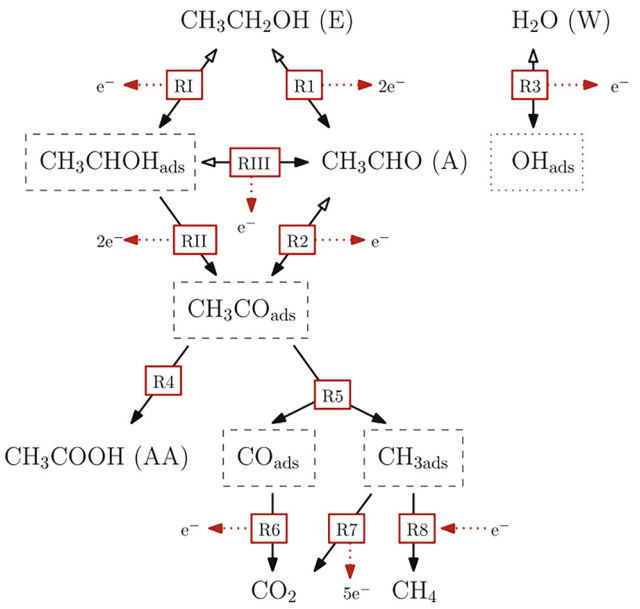

Fig. 5 Proposed reaction mechanism for the ethanol oxidation reaction on Pt based catalysts. Species adsorbed at Pt sites are indicated by a dashed box. Used with permission of Elsevier Science & Technology Journals, from a genetically optimized kinetic model for ethanol electrooxidation on Pt-based binary catalysts used in direct ethanol fuel cells, Sanchez-Monreal, P. A. Garcia-Salaberri and M. Vera, *J. Power Sources*, 2017, **363**, 341–355; permission conveyed through Copyright Clearance Center, Inc.

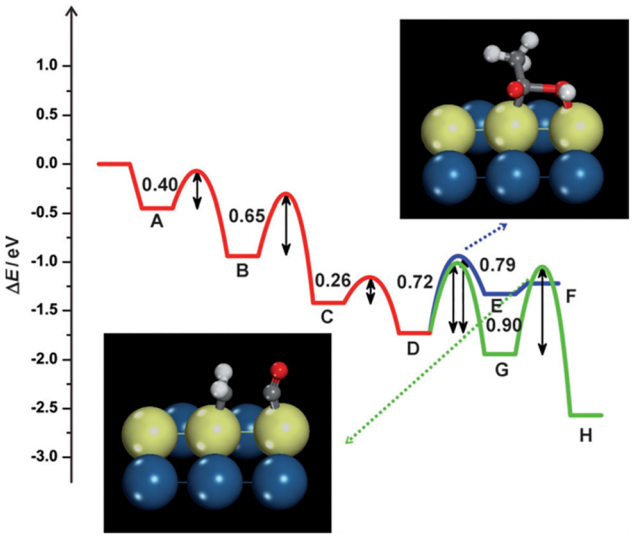

Fig. 6 Energy profiles for the minimum energy pathways for formation of acetic acid and CO_{ads} from ethanol at a Pt(211) surface. A = $CH_3CH_2OH_{ads}$, B = CH_3CHOH_{ads} C = CH_3COH_{ads}, D = CH_3CO_{ads}, E = $CH_3C(O)OH_{ads}$, F = CH_3CO_2H, G = CH_2CO_{ads}, H = CH_{2ads} + CO_{ads}. Used with permission of John Wiley & Sons – Books, origin of low CO_2 selectivity on platinum in the direct ethanol fuel cell, R. Kavanagh, X. M. Cao, W. F. Lin, C. Hardacre and P. Hu, *Angew. Chem., Int. Ed.*, 2012, **51**, 1572–1575; permission conveyed through Copyright Clearance Center, Inc.

Kavanagh *et al.*[65] calculated reaction barriers for Pt(211) (Fig. 6) that were similar to those reported by Wang and Liu.[64] However, they indicate that CO_2 formation should be competitive with acetic acid formation, which is not consistent with experimental data. To address this, and the effect of potential on selectivity, they calculated the effects of surface OH_{ads} and/or O_{ads} species that are required for both pathways. It was found that the rate of C–C bond cleavage would be decreased by two and six orders of magnitude by the presence of OH_{ads} or O_{ads}, respectively, although this would be mitigated by the presence of water.

Further understanding of the role of stepped Pt surfaces in the compete oxidation of ethanol to CO_2, demonstrated by previous experimental and computational studies, was developed by Ferre-Vilaplana *et al.*[66] FTIR and DFT results for Pt(111), Pt(553), and Pt(533) surfaces indicated that ethanol should be adsorbed in a bidentate arrangement through the carbons and that the Pt step should be free from other adsorbates.

Rizo *et al.*[67] have shown that oxidation of 1 mM ethanol at Pt(111) and Pt(100) requires the presence of OH_{ads}. Although the Pt(111) surface provided high currents, formation of CO_{ads} was not detected in voltammograms, indicating that there was not significant cleavage of the C–C bond. In contrast, Pt(100)

was less active for ethanol oxidation but produced a stripping peak for oxidation of CO_{ads}. DFT calulations elucidate the role of OH_{ads} and provide a mechanism in which OH_{ads} is involved in the formation of $CH_3CH_2O_{ads}$, which then evolves to CH_3CO_{ads}.

In addition to developing computational models of ethanol oxidation at Pt surfaces, understanding how temperature, ethanol concentration, and anode potential influence the relative rates of the reactions in Fig. 5 is crucial for controlling product distributions. Sun *et al.*[32] have presented a detailed analysis and discussion of the these effects. Since the activation energies for the complete oxidation of ethanol to CO_2 at Pt are higher than for the overall reaction (due to a higher barrier for breaking the C–C bond), selectivity for CO_2 increases with temperature. Extrapolation of their experimental data at 0.48 V to higher temperatures implies that complete conversion of 0.1 M ethanol to CO_2 would have occurred *ca.* 140 °C. A higher CO_2 selectivity observed for 0.01 M *vs.* 0.1 M ethanol was attributed to slower mass transport, which allows acetaldehyde to re-adsorb and react further to CO_2, and possibly chemical reactions of acetaldehyde. Cantane *et al.*[68] have suggested that there are dual pathways to CO_2 and acetic acid, and that adsorbed acetate may influence the effects of ethanol concentration on the product distribution.

Over the potential range most relevant to ethanol electrolysis (up to *ca.* 0.8 V), there is a complex dependence of the current on ethanol concentration, with higher currents at lower concentrations in some cases.[11,15,53,69] Accounting for changes in the product distribution with concentration, to calculate the ethanol oxidation rate, provides more reasonable dependencies, although apparent reaction orders vary greatly with concentration and potential.[11] This has been attributed to blocking of Pt surface sites by adsorbed intermediates.[69]

Yields of CO_2 generally decrease with increasing potential, which has been attributed to blocking of Pt sites by OH_{ads} and O_{ads}. This reduces the number adjacent sites available for breaking the C–C bond.[32] Evarts *et al.*[70] have shown by CO stripping experiments in an operating DEFC, and DFT calculations, that oxidative adsorption of ethanol onto a Pt(100) surface requires an ensemble of three adjacent Pt atoms. Consequently, oxidation of an increasing fraction of surface Pt sites as the potential is increased inhibits formation of CO_{ads} (ensemble effect). However, these oxidized sites promote oxidation of CO_{ads} to CO_2 and CH_3CO_{ads} to acetic acid, which increases to overall rate of ethanol oxidation. The more restrictive site requirements for breaking the C–C bond result in increasing selectivity for formation of acetic acid.

8.2. Pt alloy catalysts

For Pt based alloy catalysts (PtM), understanding how the bulk and surface compositions influence the rates of the reactions in Fig. 5 is a key challenge for the development of ethanol electrolysis technology.[61] The bulk composition influences the adsorption strength of reactants, intermediates and products primarily by electronic/ligand/charge transfer effects arising from the difference in electronegativity between Pt and M, and strain effects due to the difference in atomic radii. Both effects influence the energy of the d-band centre and adsorption energies. Higher energy d-states (relative to the Fermi level) strengthen bonding of adsorbates.[61,71–73] Combinations of more electropositive elements with Pt, and compressive strain caused by elements with smaller atomic radii than Pt, decrease the energy of the d-band centre and weaken the binding of adsorbates at Pt sites.[73]

Since CO binds strongly to Pt, weakening its adsorption by decreasing the energy of the d-band centre is a central theme in the development of more active catalysts. CO_{ads} can also be more effectively removed by oxidized surface sites of the second metal (such of Ru, Sn, Ni) through a Langmuir–Hinshelwood mechanism (eqn (4)) that is usually referred to as the bifunctional mechanism.

$$Pt–CO + M–OH \rightarrow Pt + M + CO_2 + H^+ + e^- \qquad (4)$$

Cyclic voltammetry of catalysts in aqueous acid shows the formation and reduction of surface -hydroxy and -oxy species as well as the effects of the bulk and surface composition on hydrogen adsorption and desorption. These detailed ''fingerprints''[74] of catalysts can then be correlated with their activities and selectivity for ethanol electrolysis.

8.2.1. PtRu catalysts. PtRu alloy catalysts[75] have been widely used in anodes for ethanol electrolysis and DEFC.[76] Ru decreases the energy of the d-band centre though both electronic and compressive strain effects, and is the most effective element for oxidation of CO_{ads} through the bifunctional mechanism.[73] It provides the highest currents at low potentials. However, accumulation of OH_{ads} and O_{ads} leads to lower currents than for Pt at higher potentials. In addition, PtRu alloys provide low selectivity for complete oxidation of ethanol to CO_2 and Ru dissolution is a significant concern.[77]

The differences between the electrochemical activities of PtRu and Pt for ethanol electrolysis are illustrated by the polarization curves shown in Fig. 7.[47] The PtRu catalyst provided much higher currents than Pt at potentials below 0.5 V, while currents where higher at the Pt catalyst in the mass transport limited region at higher potentials. The higher apparent mass transport rate at Pt is due to its higher selectivity for formation of CO_2 which provides a higher stoichiometry (number of electrons per ethanol molecule). Deposition of Pt onto the surface of a PtRu catalyst to form PtRu@Pt core–shell particles allows the balance between activity and selectivity to be controlled (Fig. 7).[47] The electronic and strain effects of Ru in the PtRu core are maintained, while the detrimental effects of surface Ru–OH_{ads} and Ru–O_{ads} groups at higher potentials can be mitigated.

8.2.2. PtSn catalysts. PtSn alloy catalysts have also been widely used in anodes for ethanol electrolysis and DEFC.[76,78] Although the mechanistic roles of Sn are similar to those of Ru,[79,80] controlling the activity of PtSn catalysts has been much more complex due to the formation of alloys, partially alloyed structures, and/or non-alloyed Pt–SnO_x materials, depending on the synthesis method.[78] Where comparisons are available

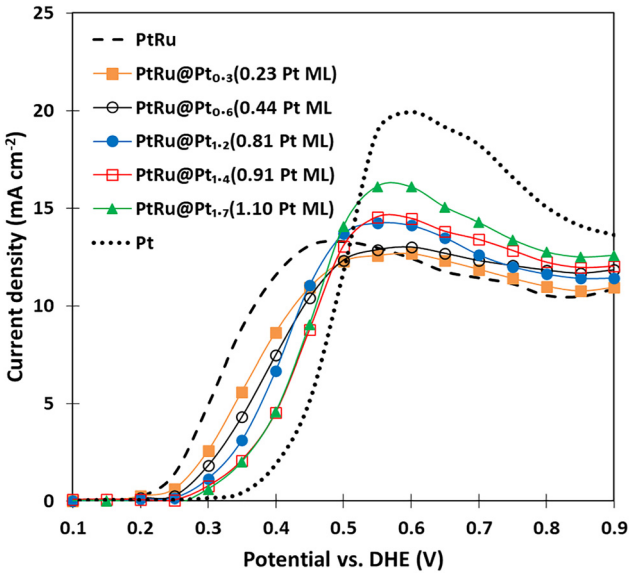

Fig. 7 Polarization curves for electrolysis of 0.1 M ethanol at PtRu, Pt and PtRu@Pt catalysts at 80 °C in crossover mode. The number of Pt monolayers (Pt ML) deposited onto the PtRh core is indicated in the legend. Adapted from ref. 47 under a Creative Commons Attribution 4.0 International License (https://creativecommons.org/licenses/by/4.0/).

for ethanol electrolysis, PtSn catalysts provide similar[37,81] or inferior[38] electrochemical performances to PtRu, and selectivity for complete oxidation of ethanol to CO_2 was higher than for PtRu.[37,38] However, the CO_2 selectivity of PtSn is much lower than for Pt.[56]

The low CO_2 selectivity of PtSn catalysts has been attributed to the combined effects of OH_{ads} and blocking of step edge sites by Sn.[56] DFT calculations show that Sn increases the barrier for C–C bond breaking at the step edge of Pt(211). In addition, Sn facilitates ethanol dehydrogenation and partial oxidation to acetaldehyde on Pt(111) and the formation of OH_{ads} for production of acetic acid.

8.2.3. PtRh catalysts. The low selectivity of PtRu and PtSn catalysts for complete oxidation of ethanol to CO_2 has led to growing interest in alloying Pt with Rh, which in contrast to Ru and Sn promotes C–C bond breaking.[29,49] PtRh catalysts have generally been found to be more active for ethanol oxidation than Pt, although this has not always been the case and depends on the composition and synthesis method.[26,82] The higher activity has been attributed to the bifunctional effect and a decrease in the energy of the d-band centre due to lattice compression.[26,83] The effects of the composition of the catalyst on activity and selectivity in aqueous electrolytes vary greatly between studies. For electrolysis of 0.1 M ethanol in a PEM cell, increasing the Rh content of the alloy was found to increase electrochemical activity and decrease selectivity for CO_2.[49] Increases in activity measured in aqueous sulphuric acid correlated with the increasing lattice strain,[49] and a similar correlation has been reported for 0.5 M ethanol.[30]

A DFT study of the effects of Ru, Sn and Rh (as well as Re and Pd) on the adsorption energy of ethanol on Pt_4M clusters through an α-hydrogen (R1 left in Fig. 5) *vs.* the O atom (R1 right) found that only Sn enhanced the α-hydrogen pathway.[84] Since adsorption through the α-hydrogen is generally the rate-determining-step, PtSn can provide higher activities for ethanol oxidation.

Sheng *et al.*[85] also found that the key intermediate was produced by α-dehydrogenation, and addressed the formation of OH_{ads}. They highlighted the significance of the subsequent β-dehydrogenation and found that the most active metals increase the rate of β-dehydrogenation but lower the potential for blocking of active sites by OH_{ads}. Rh was calculated to increase selectivity for CO_2, while Ru, Os, and Ir would decrease selectivity.

Based on FTIR and DEMS data, Galiote *et al.*[30] have proposed a reaction mechanism for ethanol oxidation at Rh rich PtRu alloys in which the presence of surface Rh atoms influences the initial ethanol dehydrogenation step. Contrary to most other models for the main pathway, ethanol is adsorbed through the oxygen atom and forms adsorbed ethoxide species.

8.2.4. Other Pt alloy catalysts. Many other Pt alloy catalysts have been shown to provide higher activities for ethanol oxidation, and in some cases higher selectivity for CO_2. Pertinent examples are provided in Table 1. Combinations of the best binary alloys with other elements provide further control of activity and selectivity. PtNi alloys are more active than Pt for ethanol oxidation due to strain, electronic and bifunctional effects, and are effective for ethanol electrolysis.[86] However, Ni is more often employed in ternary alloys such as PtRuNi, PtSnNi, and PtRhNi.[86–89] Notably, a PtRhNi catalyst has provided higher activity and selectivity for CO_2 than Pt or PtRh.[51] Fourth and fifth elements have also been employed,[90–92] with a PtRhFeNiCu intermetallic catalyst providing high performance and CO_2 selectivity in a DEFC at 200 °C.[93]

8.3. Core@shell catalysts

Further control over ethanol oxidation can be obtained by segregation of different components into different regions of the catalyst. Use of core@shell structures in which a second material is deposited onto the catalyst particles allows the effect of the core material to be combined with different effects from the shell, as illustrated in Fig. 7. In that example, the Pt shell provides high selectivity for breaking the C–C bond, while the effects of the PtRu core provide higher activities than for Pt alone. Similar effects have been induced by using Ru or Rh cores.[48,50,83] Core@shell structures can also be employed to improve the durability of the catalyst.[94]

8.4. Other catalysts with controlled structures

A wide variety of catalysts with controlled structures have been employed for ethanol oxidation including controlled shapes,[95] porous structures,[96] and single crystals to elucidate mechanisms.[97] For example, monodispersed Ga atoms on a Pt_3Mn catalyst have shown high activity and CO_2 selectivity,[98] and Pt–Sn nanosheets with preferentially exposed (100) facets have shown enhanced CO_2 selectivity.[79]

8.5. Support materials

Additional control over activity and product distribution can be provided by the material used to support the catalyst nanoparticles. Generally, the Pt-based catalysts reviewed here consist of metal nanoparticles on a high surface area carbon support such as carbon black. However, many other types of support material have been employed in order to improve activity, selectivity, and/or durability.[95] The role of the support material is an important factor in the development of advanced catalysts systems because it can provide bifunctional and/or electronic effects that complement the effects of alloying and structure control of the metal nanoparticles.

Metal oxide supports can enhance activity *via* both electronic and bifunctional effects.[31,99,100] Kowal *et al.*[31] combined PtRh nanoparticles with a Sn oxide support to produce a particularly active and selective catalyst for ethanol oxidation in aqueous perchloric acid. DFT calculations indicate that the Sn oxide support provides OH species for oxidation of CO_{ads} and inhibits OH_{ads} formation on Pt and Rh sites. This system has been developed further by a number of groups,[100] and a Pt catalyst supported on a mixed Sn–Ru oxide has been shown to provide enhanced activity and CO_2 selectivity in a DEFC.[101]

9. Evaluation and comparison of anode catalysts for ethanol electrolysis

Whereas catalysts for water electrolysis and hydrogen fuel cells can be evaluated and compared directly by using polarization curves, this is much more complex for ethanol electrolysis and DEFC because of the mixture of products that are produced. For these ethanol energy technologies, the electricity required/produced and current density are relatively minor considerations compared to the cost of ethanol, value of the products, and complexity and cost of the overall process.[11] For ethanol electrolysis, meaningful comparisons between catalysts therefore require estimates of the cost of the hydrogen produced. Although this is difficult because of the absence of a complete process model in the literature,[102,103] an approximate method for evaluating and comparing catalysts and operating conditions in this way has been used to estimate the viability of ethanol electrolysis technology.[11]

Fig. 8 shows polarization curves and cost of hydrogen plots for ethanol electrolysis at a PtRhRu catalyst based on data from ref. 11 and using a scenario in which the prices of ethanol, acetic acid, and acetaldehyde are equal. Under this scenario, low ethanol concentrations and low potentials provide the lowest hydrogen costs, which is opposite to the electrochemical performance represented by the polarization curves. However, use of Jan 2025 commodity prices (which are unlikely to represent future prices) provides a very different scenario in which there is a significant corelation between the cost of hydrogen and current densities.[11] This is due primarily to the high price of acetaldehyde resulting from high production costs and limited availability. Clearly, the optimum catalyst and operating conditions will change over time as commodity prices fluctuate, and this will require a flexible process design and a variety of catalysts that can be used to optimize cell performance and product distribution.

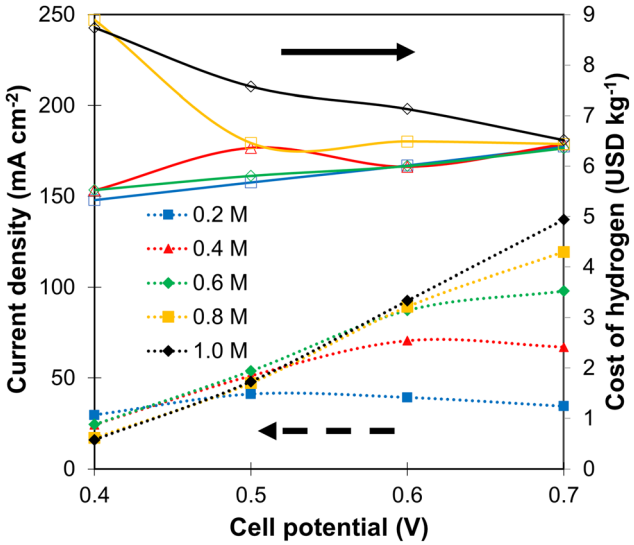

Fig. 8 Polarisation curves (bottom) and cost of hydrogen (top; scenario B in Fig. 2) *vs.* potential for electrolysis of ethanol at various concentrations at a PtRhRu catalyst. Based on data from ref. 11.

Although many different catalysts have been developed for ethanol oxidation, data for ethanol electrolysis is relatively limited, and in many cases product distributions are not reported. However, there is sufficient data available to provide adequate control of product distributions for the development of prototype processes. PtCu, PtCo, and PtNi catalyst can be used to produce acetaldehyde exclusively from 4 M ethanol (Table 1) at high current densities.[46] This would provide the best performance, and lowest cost of hydrogen based on Jan 2025 prices. However, demand for acetaldehyde is much lower than for acetic acid, and its price is volatile and uncertain.[7] PtRu at low ethanol concentrations (*e.g.* 0.1 M) and PtRhRu at moderate concentrations (0.2–1.0 M) provide high yields of acetic acid, while PtRh and PtRhNi at 0.1 M ethanol produce the highest yields of CO_2 (Table 1 and Fig. 4). Although CO_2 has little value, oxidation of ethanol to CO_2 produces the highest amount of hydrogen per ethanol molecule and so reduces the cost of ethanol. The CO_2 produced can be captured or recycled through production of ethanol from biomass.

10. Challenges and perspectives

Although development of an economically competitive ethanol electrolysis technology appears to be feasible,[11] progress is hampered by the lack of a complete model for the overall process and uncertainty in the prices of ethanol, acetic acid, and acetaldehyde. Development of a techno-economic model is essential for reliable assessment of the cost of hydrogen and its dependence on the anode catalyst and operating conditions. This will guide catalyst development and provide a methodology for objective evaluation and comparison of catalysts. Then

the wealth of knowledge on catalyst synthesis, performance, and selectivity can be used to increase current densities and refine product distributions.

In addition, catalysts that have been shown or claimed to be superior for ethanol oxidation should be rigorously tested in electrolysis cells with complete and long-term product analysis. There is little data available on catalyst durability which will become a crucial factor in the implementation of ethanol electrolysis technology. Current densities generally decrease during operation of ethanol electrolysis cells at constant potential (or potential increases at constant current) due to reversible deactivation by adsorbed intermediates,[36,104] and irreversible degradation of the catalyst over longer timescales.

Caravaca *et al.*[36] reported a *ca.* 60% decrease in current over 8 h for electrolysis of 6 M ethanol at a PtRu catalyst, at 0.8 V and 80 °C. However, the original activity was regained by cycling the potential between 0.4 and 1.1 V under the same conditions. Rodriguez-Gomez *et al.*,[45] reported more stable performance over 8 h for a PtRu catalyst at a constant current density of 100 mA cm^{-2}, with 4 M ethanol at 80 °C. Ju *et al.*[53] operated a PtSn catalyst at 0.9 V with 2 M ethanol at 70 °C for 125 h, with periodic regeneration by replacing the ethanol solution that was being recycled through the cell. The largely reversible loss of activity was attributed to the effects of acetic acid and acetaldehyde accumulation. This is a problem that will need to be addressed during process design. Post-mortem analysis of the anode catalyst layer indicated that it remained structurally stable and that there was some reduction of Sn oxides during operation of the cell.

In other PEM cell applications, Ru@Pt core–shell catalysts have been shown to be more stable than PtRu alloys because of the resistance to oxidation of Pt.[105–107] M@Pt catalysts, and particularly Rh@Pt,[94] would therefore be expected to provide improved durability relative to PtM alloys for ethanol electrolysis.

The effects of ethanol concentration on the oxidation rate and products are still not understood, and this is a fundamental problem. Separation and analysis of the rates of formation of each product[6,11,44] is required for modelling the multi-step, multi-pathway reaction mechanism.[59,63,108–110] Sánchez-Monreal *et al.*[63] have presented a comprehensive mathematical model of ethanol oxidation in a DEFC that simulates the effects of ethanol concentration. The optimum concentration of 1 M was similar to experimental values. De Oliveira *et al.*[109] modelled experimental data from DEFC with various PtSn anode catalyst compositions. Simulated surface coverages of CH_3CHO_{ads}, CH_3CO_{ads}, and OH_{ads} were similar to values measured experimentally. Pittayaporn *et al.*[110] have developed a dynamic kinetic DEFC model that includes reversible deactivation of the anode catalyst.

These models provide a crucial link between DFT calculations and experimental data, and can be adapted for optimization of catalysts[109] and operating conditions for ethanol electrolysis. However, further development is required to address the differences in mechanisms, activities and product distributions for different catalysts and catalyst compositions.[63]

Catalyst development and theoretical studies of ethanol oxidation have focused on complete oxidation of ethanol to CO_2, which has remained elusive for PEM cells. It is also debatable whether CO_2 will be the most economical product, since valorisation of acetic acid and acetaldehyde is necessary to offset the cost of ethanol.[11] Since 100% selectivity for acetaldehyde has already been achieved (Table 1), increasing acetic acid yields and current densities at low potentials appear to be the key challenges.

11. Conclusions

Production of green hydrogen from electrolysis of ethanol requires a process for separation and valorisation of by-products that allows product distributions to be optimized in response to changes in market conditions. This can be achieved by varying the ethanol concentration, cell potential, and temperature, and changing the catalyst if necessary. A wide range of catalysts have been developed and theoretical DFT and kinetic models provide a guide for optimization of product distributions. Catalysts and operating conditions should be compared and evaluated by using a cost of hydrogen analysis.

Generally, high selectivity for complete oxidation of ethanol to CO_2 is only achieved at pure Pt (or Pt rich PtRh) surfaces with low ethanol concentrations, relatively high potentials, and high temperatures. Acetic acid formation peaks at intermediate concentrations and high potentials, while acetaldehyde is the main product at high concentrations and intermediate potentials. Alloying Pt with Ru, Sn, or other oxophilic metals increases electrochemical activity (current density) but decreases selectivity for CO_2. In contrast, PtRh alloys provide high activity and CO_2 selectivity. Core–shell structures allow the benefits of an oxophilic metal to be combined with the activity, selectivity and durability of a Pt shell. Additional control of activity and selectivity can be obtained with metal oxide support materials, catalyst particles with controlled shapes and porous catalysts.

Advanced modelling of the pathways and mechanisms for electrochemical oxidation of ethanol, and anode reactions in direct ethanol fuel cells, provide a firm foundation for the development of ethanol electrolysis technology. However, process models are lacking, mitigation of the effects of recycling products though the cell has not been addressed, and the long-term durability of catalysts is unknown.

Future directions should be based on a techno-economic model that includes product separation and recycling of ethanol. They should focus on catalysts that can provide long-term stable performance and product distributions. Consequently, understanding reversible deactivation and irreversible degradation is a critical requirement. DFT calculations combined with dynamic kinetic modelling can guide the development of catalysts that are more resistant to deactivation.

Conflicts of interest

There are no conflicts to declare.

Data availability

No primary research results, software or code have been included and no new data were generated or analysed as part of this review.

Acknowledgements

This work was supported by the Natural Sciences and Engineering Research Council of Canada [grant number 2017-04260] and Memorial University.

Notes and references

1 A. Kazmi, T. Sultana, A. Ali, A. Nijabat, G. J. Li and H. W. Hou, *Energy Strategy Rev.*, 2025, **57**, 101634.
2 P. G. Pickup and E. B. Easton, *Curr. Opin. Electrochem.*, 2024, **47**, 101553.
3 E. Berretti, L. Osmieri, V. Baglio, H. A. Miller, J. Filippi, F. Vizza, M. Santamaria, S. Specchia, C. Santoro and A. Lavacchi, *Electrochem. Energy Rev.*, 2023, **6**, 30.
4 J. Wang, S. Wasmus and R. F. Savinell, *J. Electrochem. Soc.*, 1995, **142**, 4218–4224.
5 C. Lamy, E. M. Belgsir and J. M. Leger, *J. Appl. Electrochem.*, 2001, **31**, 799–809.
6 J. Kaur, R. K. Gupta and A. Kumar, *Discover Nano*, 2024, **19**, 137.
7 T. Kahlstorf, J. N. Hausmann, T. Sontheimer and P. W. Menezes, *Global Challenges*, 2023, **7**, 2200242.
8 F. S. Liu, T. P. Wang, J. J. Li, T. Wei, Z. M. Ye, D. H. Dong, B. Chen, Y. H. Ling and Z. P. Shao, *Chem. Eng. J.*, 2022, **434**, 134699.
9 C. Lamy, *J. Electroanal. Chem.*, 2020, **875**, 114426.
10 S. Ramachandran and U. Stimming, *Energy Environ. Sci.*, 2015, **8**, 3313–3324.
11 A. H. Ali and P. G. Pickup, *ACS Appl. Energy Mater.*, 2025, **8**, 13598–13606.
12 S. Rousseau, C. Coutanceau, C. Lamy and J. M. Leger, *J. Power Sources*, 2006, **158**, 18–24.
13 J. J. B. Lidasan, S. Iguchi and I. Yamanaka, *ACS Sustainable Chem. Eng.*, 2022, **10**, 2921–2929.
14 Q. Wang, G. Q. Sun, L. Cao, L. H. Jiang, G. X. Wang, S. L. Wang, S. H. Yang and Q. Xin, *J. Power Sources*, 2008, **177**, 142–147.
15 A. Rodriguez-Gomez, F. Dorado, A. de Lucas-Consuegra and A. R. de la Osa, *Fuel Process. Technol.*, 2021, **222**, 106954.
16 H. Wang, Z. Jusys and R. J. Behm, *J. Power Sources*, 2006, **154**, 351–359.
17 I. Kim, O. H. Han, S. A. Chae, Y. Paik, S. H. Kwon, K. S. Lee, Y. E. Sung and H. Kim, *Angew. Chem., Int. Ed.*, 2011, **50**, 2270–2274.
18 Y. Wang, S. Z. Zou and W. B. Cai, *Catalysts*, 2015, **5**, 1507–1534.
19 T. Iwasita and W. Vielstich, *J. Electroanal. Chem.*, 1988, **257**, 319–324.
20 L. W. H. Leung, S. C. Chang and M. J. Weaver, *J. Electroanal. Chem.*, 1989, **266**, 317–336.
21 M. H. Shao and R. R. Adzic, *Electrochim. Acta*, 2005, **50**, 2415–2422.
22 T. Iwasita and E. Pastor, *Electrochim. Acta*, 1994, **39**, 531–537.
23 H. S. Wang and H. D. Abruna, *J. Am. Chem. Soc.*, 2023, **145**, 6330–6338.
24 F. Colmati, G. Tremiliosi, E. R. Gonzalez, A. Berna, E. Herrero and J. M. Feliu, *Phys. Chem. Chem. Phys.*, 2009, **11**, 9114–9123.
25 L. Colmenares, H. Wang, Z. Jusys, L. Jiang, S. Yan, G. Q. Sun and R. J. Behm, *Electrochim. Acta*, 2006, **52**, 221–233.
26 K. Bergamaski, E. R. Gonzalez and F. C. Nart, *Electrochim. Acta*, 2008, **53**, 4396–4406.
27 A. B. Delpeuch, T. Asset, M. Chatenet and C. Cremers, *J. Electrochem. Soc.*, 2014, **161**, F918–F924.
28 A. B. Delpeuch, F. Maillard, M. Chatenet, P. Soudant and C. Cremers, *Appl. Catal., B*, 2016, **181**, 672–680.
29 J. Piwowar and A. Lewera, *J. Electroanal. Chem.*, 2020, **875**, 114229.
30 N. A. Galiote, C. A. Angelucci, V. Del Colle and G. Tremiliosi, *Electrochim. Acta*, 2025, **526**, 146084.
31 A. Kowal, M. Li, M. Shao, K. Sasaki, M. B. Vukmirovic, J. Zhang, N. S. Marinkovic, P. Liu, A. I. Frenkel and R. R. Adzic, *Nat. Mater.*, 2009, **8**, 325–330.
32 S. Sun, M. C. Halseid, M. Heinen, Z. Jusys and R. J. Behm, *J. Power Sources*, 2009, **190**, 2–13.
33 D. D. James, D. V. Bennett, G. C. Li, A. Ghumman, R. J. Helleur and P. G. Pickup, *Electrochem. Commun.*, 2009, **11**, 1877–1880.
34 A. Ghumman and P. G. Pickup, *J. Power Sources*, 2008, **179**, 280–285.
35 V. Bambagioni, M. Bevilacqua, C. Bianchini, J. Filippi, A. Lavacchi, A. Marchionni, F. Vizza and P. K. Shen, *ChemSusChem*, 2010, **3**, 851–855.
36 A. Caravaca, F. M. Sapountzi, A. de Lucas-Consuegra, C. Molina-Mora, F. Dorado and J. L. Valverde, *Int. J. Hydrogen Energy*, 2012, **37**, 9504–9513.
37 C. Lamy, T. Jaubert, S. Baranton and C. Coutanceau, *J. Power Sources*, 2014, **245**, 927–936.
38 R. M. Altarawneh and P. G. Pickup, *J. Electrochem. Soc.*, 2017, **164**, F861–F865.
39 P. Wnuk and A. Lewera, *Electrochim. Acta*, 2020, **330**, 135256.
40 D. D. James and P. G. Pickup, *Electrochim. Acta*, 2010, **55**, 3824–3829.
41 A. Jablonski, P. J. Kulesza and A. Lewera, *J. Power Sources*, 2011, **196**, 4714–4718.
42 R. M. Altarawneh, P. Majidi and P. G. Pickup, *J. Power Sources*, 2017, **351**, 106–114.
43 G. Andreadis, V. Stergiopoulos, S. Song and P. Tsiakaras, *Appl. Catal., B*, 2010, **100**, 157–164.
44 R. M. Altarawneh and P. G. Pickup, *J. Power Sources*, 2017, **366**, 27–32.
45 A. Rodriguez-Gomez, F. Dorado, A. de Lucas-Consuegra and A. R. de la Osa, *J. Energy Chem.*, 2021, **56**, 264–275.
46 A. Rodriguez-Gomez, F. Dorado, P. Sanchez and A. R. de la Osa, *J. Energy Chem.*, 2022, **70**, 394–406.
47 A. H. Ali and P. G. Pickup, *J. Electrochem. Soc.*, 2022, **169**, 034523.
48 A. H. Ali and P. G. Pickup, *ECS Adv.*, 2023, **2**, 024501.
49 A. H. Ali and P. G. Pickup, *ACS Appl. Energy Mater.*, 2025, **8**, 7450–7458.
50 A. H. Ali and P. G. Pickup, *ECS Adv.*, 2024, **3**, 034502.
51 A. H. Ali and P. G. Pickup, *Electrocatalysis*, 2025, **16**, 490–499.
52 A. Rodriguez-Gomez, E. Lepre, F. Dorado, L. Sanchez-Silva, N. Lopez-Salas and A. R. de la Osa, *Mater. Today Energy*, 2023, **32**, 101231.
53 H. Ju, S. Giddey, S. P. S. Badwal and R. J. Mulder, *Electrochim. Acta*, 2016, **212**, 744–757.
54 A. Rodríguez-Gómez, F. Dorado, A. de Lucas-Consuegra, P. Sánchez and A. R. de la Osa, *Catal. Today*, 2024, **427**, 114411.
55 J. J. B. Lidasan, Y. Kojima, S. Iguchi and I. Yamanaka, *ACS Appl. Energy Mater.*, 2024, **7**, 582–593.
56 J. M. Jin, T. Sheng, X. Lin, R. Kavanagh, P. Hamer, P. J. Hu, C. Hardacre, A. Martinez-Bonastre, J. Sharman, D. Thompsett and W. F. Lin, *Phys. Chem. Chem. Phys.*, 2014, **16**, 9432–9440.
57 A. B. Delpeuch, T. Asset, M. Chatenet and C. Cremers, *Fuel Cells*, 2015, **15**, 352–360.
58 A. R. Fairhurst, J. Snyder, C. Wang, D. Strmcnik and V. R. Stamenkovic, *Chem. Rev.*, 2025, **125**, 1332–1419.
59 J. Sanchez-Monreal, P. A. Garcia-Salaberri and M. Vera, *J. Power Sources*, 2017, **363**, 341–355.
60 H. A. Asiri and A. B. Anderson, *J. Electrochem. Soc.*, 2015, **162**, F115–F122.
61 D. J. Zheng, J. Y. Peng, K. McCormack, H. B. Xu, J. S. Kang, Z. S. Wang, Z. C. Ren, J. Li, Y. Román-Leshkov and Y. Shao-Horn, *EES Catal.*, 2024, **2**, 1186–1209.
62 J. Florez-Montano, G. Garcia, O. Guillen-Villafuerte, J. L. Rodriguez, G. A. Planes and E. Pastor, *Electrochim. Acta*, 2016, **209**, 121–131.
63 J. Sanchez-Monreal, P. A. Garcia-Salaberri and M. Vera, *Appl. Energy*, 2019, **251**, 113264.
64 H. F. Wang and Z. P. Liu, *J. Am. Chem. Soc.*, 2008, **130**, 10996–11004.
65 R. Kavanagh, X. M. Cao, W. F. Lin, C. Hardacre and P. Hu, *Angew. Chem., Int. Ed.*, 2012, **51**, 1572–1575.
66 A. Ferre-Vilaplana, C. Buso-Rogero, J. M. Feliu and E. Herrero, *J. Phys. Chem. C*, 2016, **120**, 11590–11597.
67 R. Rizo, A. Ferre-Vilaplana, E. Herrero and J. M. Feliu, *ACS Sustainable Chem. Eng.*, 2023, **11**, 4960–4968.
68 D. A. Cantane and E. R. Gonzalez, *J. Electrochem. Soc.*, 2012, **159**, B355–B359.

69 A. Sayadi and P. G. Pickup, *Electrochim. Acta*, 2016, **215**, 84–92.
70 S. E. Evarts, I. Kendrick, B. L. Wallstrom, T. Mion, M. Abedi, N. Dimakis and E. S. Smotkin, *ACS Catal.*, 2012, **2**, 701–707.
71 B. Hammer and J. K. Norskov, *Surf. Sci.*, 1995, **343**, 211–220.
72 J. K. Norskov, F. Abild-Pedersen, F. Studt and T. Bligaard, *Proc. Natl. Acad. Sci. U. S. A.*, 2011, **108**, 937–943.
73 M. A. Rigsby, W. P. Zhou, A. Lewera, H. T. Duong, P. S. Bagus, W. Jaegermann, R. Hunger and A. Wieckowski, *J. Phys. Chem. C*, 2008, **112**, 15595–15601.
74 E. N. El Sawy, H. A. El-Sayed and V. I. Birss, *Chem. Commun.*, 2014, **50**, 11558–11561.
75 Y. V. Tolmachev and O. A. Petrii, *J. Solid State Electrochem.*, 2017, **21**, 613–639.
76 A. Q. K. Nguyen, H. Q. Pham, S. T. M. Huynh and T. T. Huynh, *Adv. Sustainable Syst.*, 2023, **7**, 2300205.
77 E. Antolini, *J. Solid State Electrochem.*, 2011, **15**, 455–472.
78 E. Antolini and E. R. Gonzalez, *Catal. Today*, 2011, **160**, 28–38.
79 Z. P. Zheng, Y. Z. Xu, W. Yan, Y. C. Sun, Q. R. Jiang, Q. Kuang and Z. X. Xie, *J. Phys. Chem. C*, 2023, **127**, 11875–11882.
80 L. Calvillo, L. M. De Leo, S. J. Thompson, S. W. T. Price, E. J. Calvo and A. E. Russell, *J. Electroanal. Chem.*, 2018, **819**, 136–144.
81 A. R. de la Osa, A. B. Calcerrada, J. L. Valverdea, E. A. Baranova and A. de Lucas-Consuegra, *Appl. Catal., B*, 2015, **179**, 276–284.
82 S. Sen Gupta and J. Datta, *J. Electroanal. Chem.*, 2006, **594**, 65–72.
83 F. H. B. Lima and E. R. Gonzalez, *Appl. Catal., B*, 2008, **79**, 341–346.
84 Z. F. Xu and Y. Wang, *J. Phys. Chem. C*, 2011, **115**, 20565–20571.
85 T. Sheng, W. F. Lin, C. Hardacre and P. Hu, *Phys. Chem. Chem. Phys.*, 2014, **16**, 13248–13254.
86 E. Antolini, *Energies*, 2017, **10**, 42.
87 S. Beyhan, C. Coutanceau, J. M. Leger, T. W. Napporn and F. Kadirgan, *Int. J. Hydrogen Energy*, 2013, **38**, 6830–6841.
88 S. Beyhan, J. M. Leger and F. Kadirgan, *Appl. Catal., B*, 2013, **130**, 305–313.
89 G. X. Yang, Q. Zhang, H. Yu and F. Peng, *Particuology*, 2021, **58**, 169–186.
90 M. Ammam and E. B. Easton, *J. Power Sources*, 2012, **215**, 188–198.
91 G. R. Salazar-Banda, K. I. B. Eguiluz, M. M. S. Pupo, H. B. Suffredini, M. L. Calegaro and L. A. Avaca, *J. Electroanal. Chem.*, 2012, **668**, 13–25.
92 R. M. Altarawneh, *Ionics*, 2025, 9509–9523.
93 D. D. Wang, Z. W. Chen, Y. J. Wu, Y. C. Huang, L. Tao, J. Chen, C. L. Dong, C. V. Singh and S. Y. Wang, *SmartMat*, 2023, **4**, e1117.
94 M. Vega-Paredes, R. Aymerich-Armengol, D. A. Esteban, S. Marti-Sanchez, S. Bals, C. Scheu and A. G. Manjon, *ACS Nano*, 2023, **17**, 16943–16951.
95 L. Yaqoob, T. Noor and N. Iqbal, *RSC Adv.*, 2021, **11**, 16768–16804.
96 A. K. Ipadeola, K. Eid, A. K. Lebechi, A. M. Abdullah and K. I. Ozoemena, *Electrochem. Commun.*, 2022, **140**, 107330.
97 R. Rizo, S. Perez-Rodriguez and G. Garcia, *ChemElectroChem*, 2019, **6**, 4725–4738.
98 Y. Wang, M. Zheng, Y. R. Li, C. L. Ye, J. Chen, J. Y. Ye, Q. H. Zhang, J. Li, Z. Y. Zhou, X. Z. Fu, J. Wang, S. G. Sun and D. S. Wang, *Angew. Chem., Int. Ed.*, 2022, e202115735.
99 R. B. Moghaddam and P. G. Pickup, *Electrochim. Acta*, 2012, **65**, 210–215.
100 N. S. Marinkovic, M. Li and R. R. Adzic, *Top. Curr. Chem.*, 2019, **377**, 11.
101 D. D. James, R. B. Moghaddam, B. Y. Chen and P. G. Pickup, *J. Electrochem. Soc.*, 2018, **165**, F215–F219.
102 N. Gutiérrez-Guerra, M. Jiménez-Vázquez, J. C. Serrano-Ruiz, J. L. Valverde and A. de Lucas-Consuegra, *Chem. Eng. Process.*, 2015, **95**, 9–16.
103 B. Caglar, M. Araz, H. G. Ozcan, A. Calisan and A. Hepbasli, *Int. J. Hydrogen Energy*, 2021, **46**, 12615–12638.
104 A. Caravaca, A. de Lucas-Consuegra, A. B. Calcerrada, J. Lobato, J. L. Valverde and F. Dorado, *Appl. Catal., B*, 2013, **134**, 302–309.
105 J. Xie, Q. H. Zhang, L. Gu, S. Xu, P. Wang, J. G. Liu, Y. Ding, Y. F. Yao, C. W. Nan, M. Zhao, Y. You and Z. G. Zou, *Nano Energy*, 2016, **21**, 247–257.
106 A. G. Manjon, M. Vega-Paredes, V. Berova, T. Gansler, T. Schwarz, N. A. R. Rivas, K. Hengge, T. Jurzinsky and C. Scheu, *Nanoscale*, 2022, **14**, 18060–18069.
107 V. Berova, A. G. Manjon, M. V. Paredes, T. Schwarz, N. A. Rivas, K. Hengge, T. Jurzinsky and C. Scheu, *J. Power Sources*, 2023, **554**, 232327.
108 M. Meyer, J. Melke and D. Gerteisen, *Electrochim. Acta*, 2011, **56**, 4299–4307.
109 D. de Oliveira, F. Colmati and R. de Sousa, Jr., *Energies*, 2022, **15**, 9143.
110 N. Pittayaporn, A. Therdthianwong, S. Therdthianwong and R. Songprakorp, *Int. J. Energy Res.*, 2019, **43**, 2615–2634.